International Journal of Research in Engineering and Science (IJRES)
ISSN (Online): 2320-9364, ISSN (Print): 2320-9356
www.ijres.org Volume 12 Issue 9 ǁ September 2024 ǁ PP. 51-63

Application of Special Plier Type Gripper with Spherical Robot Arm

Ziya ÖZÇELİK [1*], Muhammet Mevlüt KARACA [2]
[*1]*Department of Mechatronic Engineering, University of Selcuk, Türkiye*
[2]*Department of Mechanical Engineering, University of Karabük, Türkiye*
Corresponding Author: Ziya ÖZÇELİK

Abstract
Robotic arms, which are an important part of the industry, have developed in parallel with technology. Robot arms, which generally work in repetitive jobs and areas that will put human health at risk, increase the quality and speed in the industry. This study involves the design of a pneumatic end-effector (gripper) robotic arm developed for grasping 2-axis, spherical, and special cylindrical and ear-shaped objects. The assembly was performed using CAD software and a simulation was carried out. After addressing assembly issues, the manufacturing was completed. Installation of mechanical and electrical equipment has been completed. Then, microcontroller connections were made, and the robot arm was made operational. The Denavit-Hartenberg method was used to determine the coordinate values of the end-effector and to perform the forward kinematic calculations of the robotic arm. Inverse kinematic calculations were also performed to determine the joint angle values required for the end-effector to reach the target coordinate values. A control program for the robotic arm was written using the Arduino-Uno microcontroller. The kinematic equations obtained were incorporated into the program. Encoder data was read via a serial (com) port using Matlab connected to the Arduino that drives the robotic arm. The control of the robotic arm was achieved using the equations in the program. Tests were conducted to assess the repeatability and accuracy of the robotic arm controlled by the microcontroller. Simultaneous data read from the encoder during experimental results were recorded and compared with theoretical data.

Keywords: *Spherical Robot, Gripper Design, Robot Kinematics, Robot Dynamics, Trajectory Planning, Industrial Robotic Arm.*

Date of Submission: 01-09-2024 Date of acceptance: 11-09-2024

I. INTRODUCTION

Robotic arms, which are indispensable components of the industry, provide significant advantages in quality and mass production. With a wide range of applications, robotic arms are used across various sectors including automotive, food, textile, chemical industries, as well as in space, medical, and military fields. The advanced technological equipment of robotic arms makes it challenging to use and manufacture them in developing countries. Ready-made systems available externally also pose cost challenges. When examined as a process, robotic arms stand out with features such as welding, painting, gluing, assembly, transportation, and packaging. It is important to manufacture these systems within our country's industry using available resources. In this context, the design, manufacturing, and analysis steps of the robotic arm have been addressed from many aspects. In the manufacturing stage of a product, it needs to be transported from one place to another to proceed through stages such as production, assembly, packaging, and storage. During the transportation phase, the robot's primary applications involve moving the object along a predetermined path without causing any physical changes and then releasing it (Siciliano et al., 2009). The most comprehensive definition of an industrial robot arm, according to the ISO 8373 standard, is that it is a fixed or mobile, automatic or controlled, reprogrammable, multipurpose manipulator that is programmable on three or more axes for use in industrial automation applications. ("ISO 8373:2012(en), Robots and robotic devices—Vocabulary", n.d.) A 3-dimensional simulation of the Movemaster EX (RV-M1) industrial robot, developed by Mitsubishi, has been carried out in a computer environment. This simulation was used to study the movement behavior of the robot arm, detect potential errors, and observe the effects of modifications. (Adalı, 2001) The joint angle values required for the robotic arm to reach the object were calculated through inverse kinematics and sent to the robotic arm via a microprocessor. The control software was implemented using the Arduino Mega 2560 microcontroller board (Yavuz, Alıcı, and Uyar, 2015). The design of the SCARA type robot was modeled in Solidworks, and the parts were manufactured using CNC machining codes. Inverse and forward kinematic calculations were performed and simulated in Matlab (Saygılı, 2006). The kinematic and dynamic calculations

and controls of the ABB IRB 140 industrial robot were performed. An adaptive control system was developed and the Denavit-Hartenberg method was used through Matlab (Öztürk, 2014). The use of homogeneous transformations and Lagrangian mechanics formulation facilitates the derivation, analysis, and simplification of complex robot dynamic equations (Bejczy and Paul, 1981). The control performance of a three-degree-of-freedom robotic arm under force effects was compared using PID and fuzzy logic methods in a Matlab-Simulink simulation environment (Kayışlı and Uğur, 2017).

In this study, the design, manufacturing, and analysis of a two-axis, spherical trajectory-tracing industrial robotic arm with a special pneumatic end-effector have been carried out. This robotic arm features a different design compared to existing robotic arms in the literature. This difference appears in two distinct aspects of the design: the special end-effector and the pulley system. The robotic arm is equipped with a special pulley system starting from the second axis. This setup ensures that the part held by the end-effector remains parallel to the ground, effectively serving as a third axis. An angular pneumatic design was developed for the end-effector to grasp cylindrical and ear-shaped objects. Two AC servo motors were used in the robotic arm to achieve axis movements and were driven by PWM signals with PID control through the Arduino Uno microcontroller.

II. MATERIALS AND METHODS

In this study, it is aimed to design a robot arm with a spherical working space, a pick-and-place task, and a special angular motion mechanism and an end holder element to grasp conical and eared objects. The design was created using Solidworks, a computer-aided solid modeling program, and simulations were conducted to resolve assembly issues. Rotational hinge joints were used in the axes. The robotic arm is driven by two AC permanent magnet synchronous servo motors. Additionally, since the robotic arm will be used in an industrial environment, the motors have been selected to be IP67 certified, making them resistant to water, dust, and impacts. To increase the output torque of the servo motors and enable the robotic arm to lift heavier loads, two planetary gear reducers were used.

The general appearance of the solid model of the robotic arm used in this study is shown in Figure 1

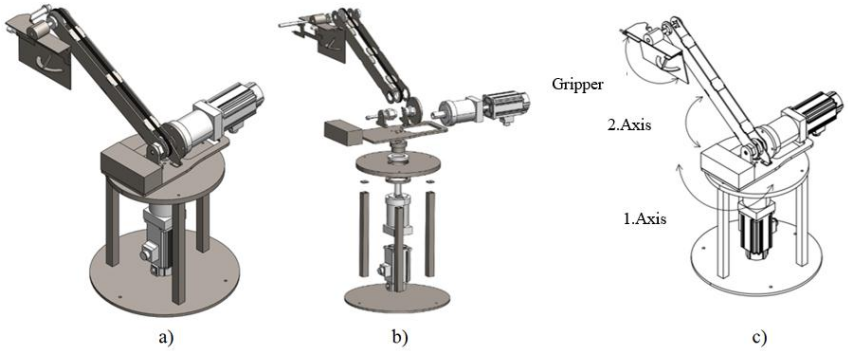

Figure 1: a) General virtual view of the robotic arm b) Exploded assembly view of the robotic arm c) Axes and end-effector

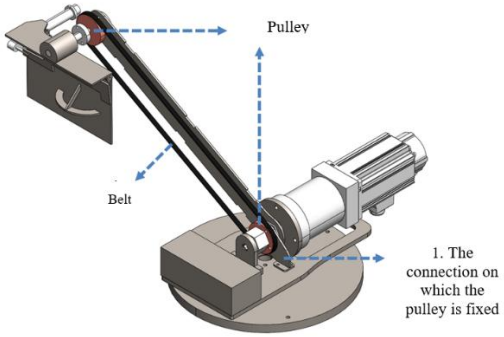

Figure 2: Belt Pulley System

As shown in Figure 2, a belt and pulley system, which is one of the direct transmission systems, has been used in the section of the robot from the second axis to the end-effector. In this system, the first pulley is fixed, while the second pulley is mounted on bearings and is movable. The advantage of the belt and pulley system over a chain drive system is its lightweight and quiet operation.

Figure 3: Assembled outer casing of the robotic arm

After addressing assembly issues in the virtual environment, the manufacturing phase of the robotic arm began. St52 material was chosen for the body section. The properties of the material will be discussed in subsequent sections. The plates, which were cut using a laser, were assembled with connection elements and welding. Electrostatic paint was applied to prevent corrosion and improve aesthetics. The body of the assembled robotic arm is shown in Figure 3.

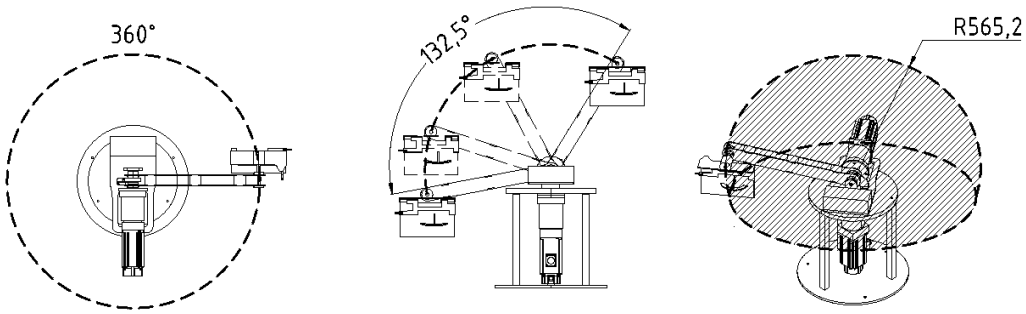

Figure 4. Boundary conditions of the axes of the robotic arm

Figure 4 shows the boundary conditions of the robotic arm. While the first axis can rotate 360°, the second axis has a rotation capability of 132.5°. The system has a spherical working area with a radius of 565.2 mm.

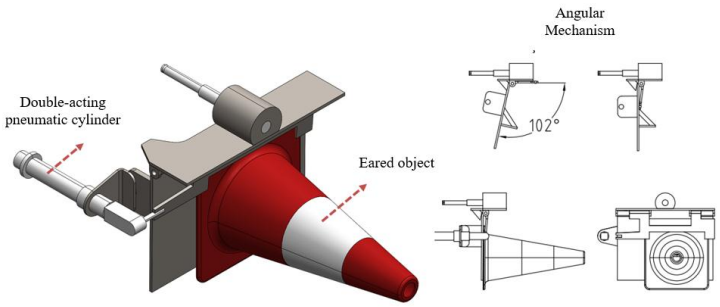

Figure 5: End-effector

A mechanism that works with an angular movement and an open-close logic was used in the robot arm. This mechanism is driven by a double-acting cylinder. It is intended to grasp objects with ears. A general visual and mechanism operating logic of the pneumatic end-operator are shown in Figure 5. The most important feature of the designed end-effector is its ability to maintain the object parallel to the ground in the same orientation it was originally picked up, while transporting it from one location to another, as illustrated in Figure 6. In this way, it is possible to place the object at the desired target without disturbing its position.

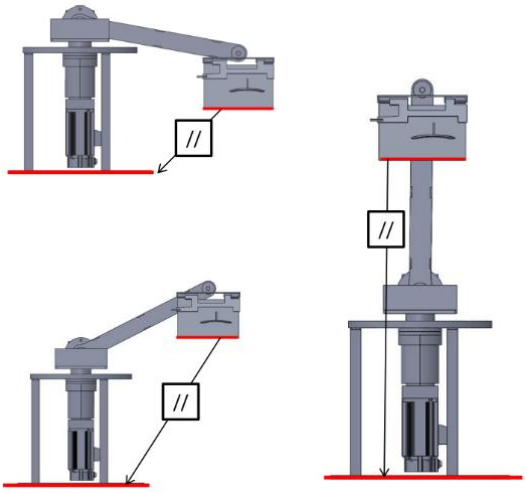

Figure 6: Parallelism of the robot arm gripper to the ground during movement.

Parallelism process is carried out with a belt pulley system. Additionally, the belt and pulley system allow the same task to be performed using only two axes instead of three, thereby conserving one axis. Different end function models can be adapted to this designed robot arm according to the desired work.

2.1 Material selection

St 52 material, which is the steel type, was selected for the overall body of the robot arm. The reason why this steel is called St52 is that it has a tensile strength of 52 kg/mm. In addition, the welding performance of these steels is high. It is usually used in normal machine parts, crane, chassis, bridges and mobile equipment.

2.2 Motor selection

In the selection of the motor, the selection was made by considering the amount of load to be lifted by the robot arm, sensitivity, usability and controllability parameters in the industry. The technical information of the two AC servo motors and gearboxes used in the robot arm with the same characteristics are shown in Tables 1 and 2.

Table 1. Features of AC Servo motor used

Axis	Motor Type	Engine Power (kW)	Velocity (dev/dk)	Motor Torque (N.m)
1 ve 2	Panasonic Minas A5 (MSME204G1G)	2	3000	6,37

Table 2. Gearbox features used

Reducer Type	Reducer Ratio
Planetary Gear Reducer (Apex Dynamics PEII120)	1/25

2.3 Assembly of the board and microcontroller

The placement and assembly of electrical elements such as drivers, power supply, fuses, LED, 3-phase switch and fan of AC servo motors in the robot arm in the virtual environment in the panel are shown in Figure 7 and Figure 8.

Figure 7: Panel assembled

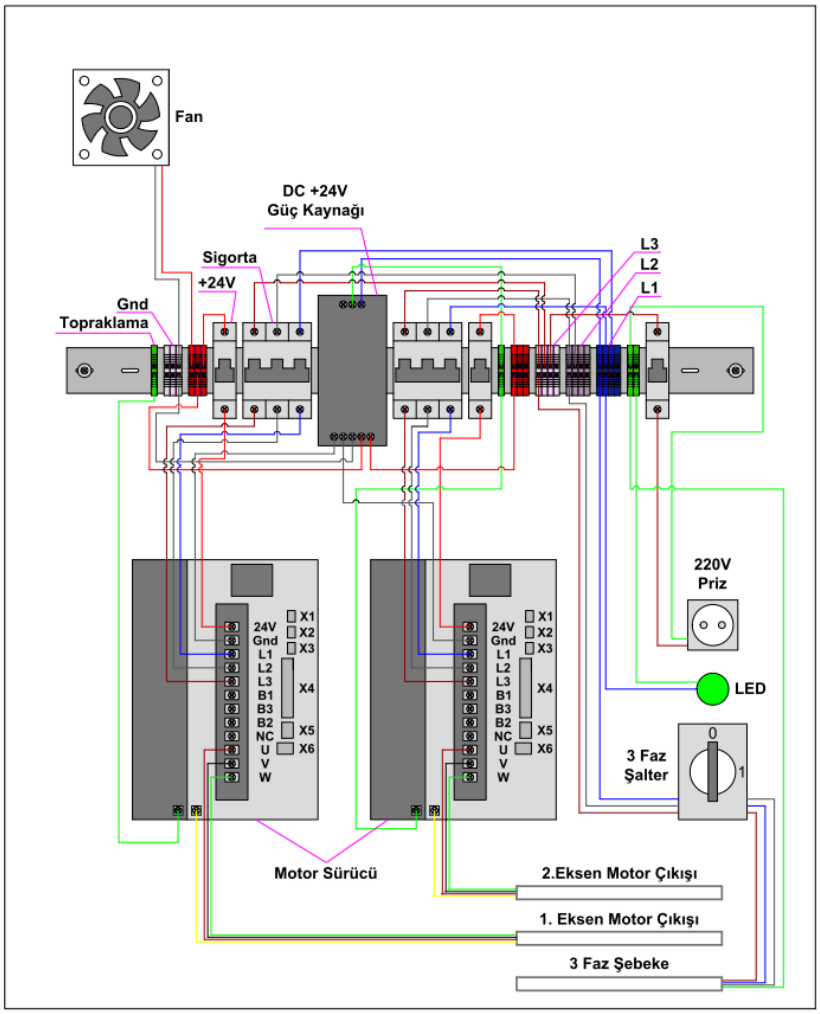

Figure 8: Layout diagram of board elements

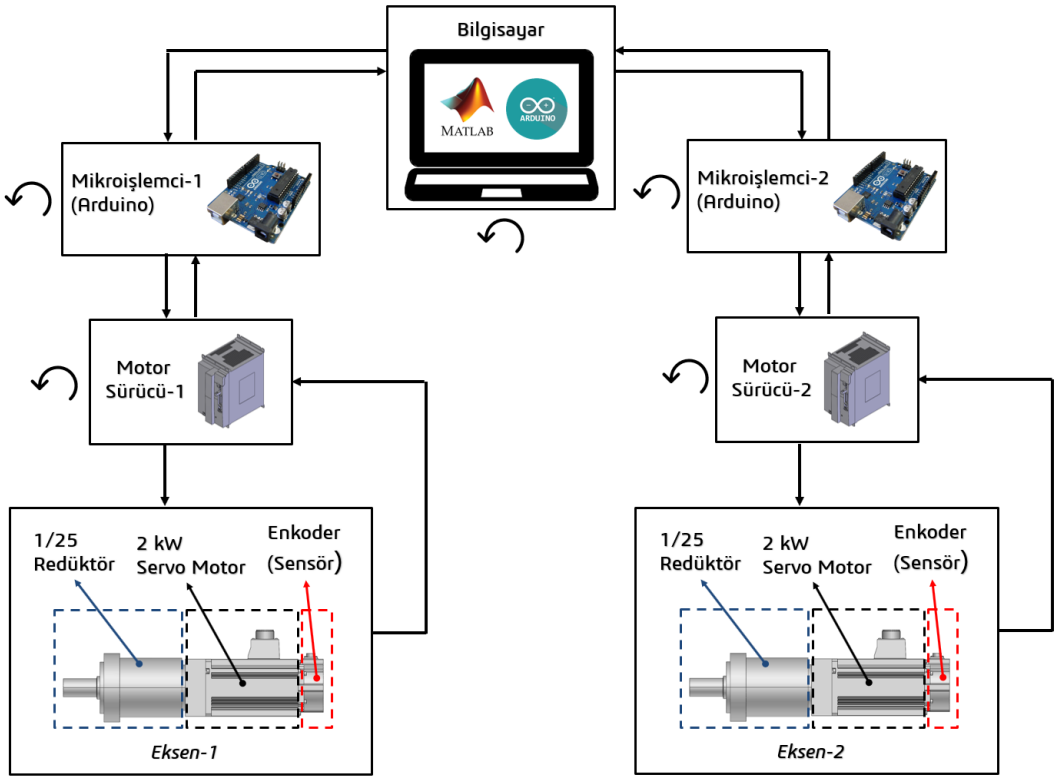

Figure 9: Control scheme

Figure 9 shows the control diagram of the system. The location information sent from the computer via the Matlab interface is transmitted to the motor driver with Arduino. After motor driver positions of the motor, feedback is provided from the encoder to the Arduino. After the encoder information is processed in Arduino, feedback is given back to the Matlab interface on the computer. Incoming information is converted into graphics by storing data in Matlab.

2.4 Straight (forward) kinematic calculations of the designed robot arm

The simplified version of the designed two-axis robot arm is shown in Figure 10 to make the axis assignments easier to understand. The axes consist of rotating joints. There is a 90° angle between the first joint and the axis of rotation of the second joint. Since there is a pulley transfer system from the second joint to the third joint, θ2 is dependent on θ3 and rotates in opposite directions with each other.

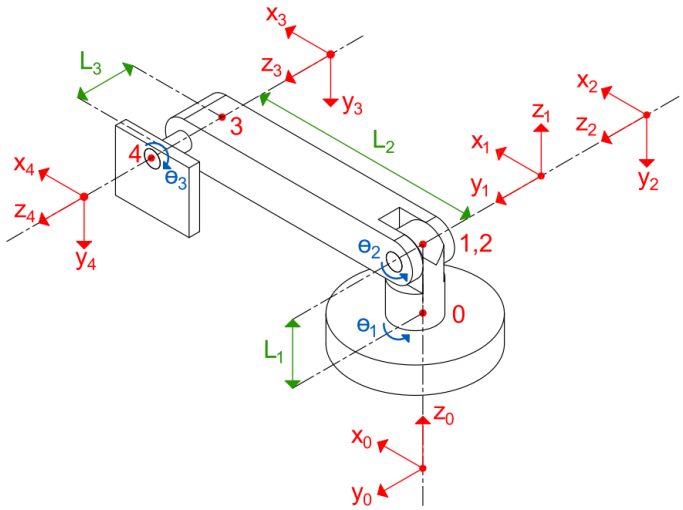

Figure 10. Designed robot arm axis assignments

After the axis assignments of the designed robot arm are made, the D-H parameters are given in Table 3.

Tablo 3: D-H parametreleri tablosu

Axis No	**D-H Variables**			
İ	α_{i-1}	a_{i-1}	d_i	θ_i
1	0°	0	L_1	θ_1
2	-90°	0	0	θ_2
3	0°	L_2	0	0°
4	0°	0	L_3	$\theta_3 = -\theta_2$

After the table is created, the following calculations are followed in order:
D-H variables are found.

$$\alpha_0 = 0, \alpha_1 = -\frac{\pi}{2}, \alpha_2 = 0, \alpha_3 = 0$$
$$a_0 = 0, a_1 = 0, a_2 = L_2, a_3 = 0$$
$$d_1 = L_1, d_2 = 0, d_3 = 0, d_4 = L_3$$
$$\theta_1 = \theta_1, \theta_2 = \theta_2, \theta_3 = 0, \theta_4 = -\theta_2 \quad (1)$$

Joint transformation matrices are created.

$$ {}^{0}_{1}T = \begin{bmatrix} cos\theta_1 & -sin\theta_1 & 0 & 0 \\ sin\theta_1 & cos\theta_1 & 0 & 0 \\ 0 & 0 & 1 & L_1 \\ 0 & 0 & 0 & 1 \end{bmatrix}$$
$$ {}^{1}_{2}T = \begin{bmatrix} cos\theta_2 & -sin\theta_2 & 0 & 0 \\ 0 & 0 & 1 & 0 \\ -sin\theta_2 & -cos\theta_2 & 0 & 0 \\ 0 & 0 & 0 & 1 \end{bmatrix}$$
$$ {}^{2}_{3}T = \begin{bmatrix} 1 & 0 & 0 & L_2 \\ 0 & 1 & 0 & 0 \\ 0 & 0 & 1 & 0 \\ 0 & 0 & 0 & 1 \end{bmatrix}$$
$$ {}^{3}_{4}T = \begin{bmatrix} cos\theta_2 & sin\theta_2 & 0 & 0 \\ -sin\theta_2 & cos\theta_2 & 0 & 0 \\ 0 & 0 & 1 & L_3 \\ 0 & 0 & 0 & 1 \end{bmatrix} \quad (2)$$

${}^{0}_{4}T$ forward-directional robot kinematics are generated from the main frame to the vehicle frame.

$$ {}^{0}_{4}T = \begin{bmatrix} cos\theta_1 & 0 & -sin(\theta_1) & -sin(\theta_1)L_3 + cos(\theta_1)cos(\theta_2)L_2 \\ sin\theta_1 & 0 & cos\theta_1 & cos(\theta_1)L_3 + sin(\theta_1)cos(\theta_2)L_2 \\ 0 & -1 & 0 & -sin(\theta_2)L_2 + L_1 \\ 0 & 0 & 0 & 1 \end{bmatrix} \quad (3)$$

The position vectors in the ${}^{0}_{4}T$ transformation matrix are constructed as shown in Equation 4 with their elements in the third column of the matrix in Equation 3.

$$P_x = -sin(\theta_1)L_3 + cos(\theta_1)cos(\theta_2)L_2$$
$$P_y = cos(\theta_1)L_3 + sin(\theta_1)cos(\theta_2)L_2$$
$$P_z = -sin(\theta_2)L_2 + L_1 \quad (4)$$

2.5 Inverse kinematic analytical solution

In inverse kinematics, the angle values that should be given to the joints are calculated according to the position and orientation information of the end effector. Calculations used from inverse kinematics are not linear and can be complex. Therefore, there can be more than one set of solutions.

The advanced kinematics of the six degrees of freedom robot arm are shown in Equation 5. Equation 6 shows the matrix containing the position and orientation information of its matrix ${}^{0}_{6}\mathrm{T}$.

$$ {}^{0}_{6}T = {}^{0}_{1}T\ {}^{1}_{2}T\ {}^{2}_{3}T\ {}^{3}_{4}T\ {}^{4}_{5}T\ {}^{5}_{6}T \tag{5} $$

$$ {}^{0}_{6}T = \begin{bmatrix} r_{11} & r_{12} & r_{13} & p_x \\ r_{21} & r_{22} & r_{23} & p_y \\ r_{31} & r_{32} & r_{33} & p_z \\ 0 & 0 & 0 & 1 \end{bmatrix} \tag{6} $$

The equation in Equation 5 is multiplied by $[{}^{0}_{1}\mathrm{T}]^{-1}$ on both sides, as shown in Equation 7. Since the product of a matrix and its inverse equals the identity matrix, this results in $[{}^{0}_{1}\mathrm{T}]^{-1}\ {}^{0}_{1}\mathrm{T} = \mathrm{I}$. The rearranged form of the equation is shown in Equation 8.

$$ [{}^{0}_{1}T]^{-1}\ {}^{0}_{6}T = [{}^{0}_{1}T]^{-1}\ {}^{0}_{1}T\ {}^{1}_{2}T\ {}^{2}_{3}T\ {}^{3}_{4}T\ {}^{4}_{5}T\ {}^{5}_{6}T \tag{7} $$

$$ [{}^{0}_{1}T]^{-1}\ {}^{0}_{6}T = {}^{1}_{2}T\ {}^{2}_{3}T\ {}^{3}_{4}T\ {}^{4}_{5}T\ {}^{5}_{6}T \tag{8} $$

In inverse kinematics, the solution is made by multiplying and equalizing the transformation matrices from the right and left sides, respectively. Repeated versions of these operations are shown in Equation 9.

$$ \begin{gathered} [{}^{0}_{1}T\ {}^{1}_{2}T\ ]^{-1}\ {}^{0}_{6}T = {}^{2}_{3}T\ {}^{3}_{4}T\ {}^{4}_{5}T\ {}^{5}_{6}T \\ [{}^{0}_{1}T\ {}^{1}_{2}T\ {}^{2}_{3}T]^{-1}\ {}^{0}_{6}T = {}^{3}_{4}T\ {}^{4}_{5}T\ {}^{5}_{6}T \\ [{}^{0}_{1}T\ {}^{1}_{2}T\ {}^{2}_{3}T\ {}^{3}_{4}T]^{-1}\ {}^{0}_{6}T = {}^{4}_{5}T\ {}^{5}_{6}T \\ [{}^{0}_{1}T\ {}^{1}_{2}T\ {}^{2}_{3}T\ {}^{3}_{4}T\ {}^{4}_{5}T\ ]^{-1}\ {}^{0}_{6}T = {}^{5}_{6}T \end{gathered} \tag{9} $$

The main trigonometric formulas used in inverse kinematics are:

$$ cos\,\theta = a \quad ise \quad \theta = Atan2\left(\sqrt{1-a^2}, a\right) \tag{10} $$

$$ sin\theta = a \quad ise \quad \theta = arctan2\left(a, \pm\sqrt{1-a^2}\right) \tag{11} $$

$$ cos\theta = a \quad ve \quad sin\theta = b \quad ise \quad \theta = arctan2b, a \tag{12} $$

$$ a\,sin\theta + b\,cos\,\theta = 0 \quad ise $$
$$ \theta = arctan2(-b, a) \quad veya \quad arctan2(b, -a) \tag{13} $$

$$ asin\theta + bcos\theta = c \quad ise $$
$$ \theta = arctan2(a, b) + arctan(\pm\sqrt{a^2 + b^2 - c^2}, c) \tag{14} $$

To obtain the inverse of a transformation matrix, the first step is to compute the transpose of the rotation matrix. Then, the position vector and the matrix transposed are multiplied and a minus sign is placed in front of it. These calculated values are written in their places in Equation 15 and the inverse of the matrix is found.

$$ [{}^{N-1}_{N}T]^{-1} = \begin{bmatrix} ({}^{N-1}_{N}R)^T & -({}^{N-1}_{N}R)^T P_N \\ 0\ 0\ 0 & 1 \end{bmatrix} \tag{15} $$

In the inverse kinematic calculation of the designed robot arm, the following steps were followed respectively: The rotation matrix of the first addition was created.

$$ {}^{0}_{1}R = \begin{bmatrix} cos(\theta_1) & -sin(\theta_1) & 0 \\ sin(\theta_1) & cos(\theta_1) & 0 \\ 0 & 0 & 1 \end{bmatrix} \tag{16} $$

Transpose of rotation matrix.

$$ ({}^{0}_{1}R)^T = \begin{bmatrix} cos(\theta_1) & sin(\theta_1) & 0 \\ -sin(\theta_1) & cos(\theta_1) & 0 \\ 0 & 0 & 1 \end{bmatrix} \tag{17} $$

The position vector for the first addition has been created.

$$ {}^{0}_{1}P = \begin{bmatrix} 0 \\ 0 \\ L_1 \end{bmatrix} \tag{18} $$

The transpose of the rotation matrix of the first addition was multiplied by the position vector.

$$ ({}^{0}_{1}R)^T . {}^{0}_{1}P = \begin{bmatrix} 0 \\ 0 \\ -L_1 \end{bmatrix} \tag{19} $$

The data obtained is substituted in Equation 15 and the inverse of the transformation matrix of the first addition is created as shown in Equation 20.

$$ ({}^{0}_{1}T)^{-1} = \begin{bmatrix} cos\theta_1 & sin\theta_1 & 0 & 0 \\ -sin\theta_1 & cos\theta_1 & 0 & 0 \\ 0 & 0 & 1 & -L_1 \\ 0 & 0 & 0 & 1 \end{bmatrix} \tag{20} $$

Equation 20 is obtained by multiplying the matrix created in Equation 21 by both sides of the equation in the forward direction kinematic equation of the robot arm.

$$ [{}^{0}_{1}T]^{-1} \, {}^{0}_{4}T = [{}^{0}_{1}T]^{-1} \, {}^{0}_{1}T \, {}^{1}_{2}T \, {}^{2}_{3}T \, {}^{3}_{4}T \tag{21} $$

The calculation on the left side of the equation in Equation 21 is shown in Equation 22. The inverse of the first joint is multiplied by the matrix representing the forward direction kinematics.

$$ ({}^{0}_{1}T)^{-1} . {}^{0}_{4}T = \begin{bmatrix} cos\theta_1 & sin\theta_1 & 0 & 0 \\ -sin\theta_1 & cos\theta_1 & 0 & 0 \\ 0 & 0 & 1 & -L_1 \\ 0 & 0 & 0 & 1 \end{bmatrix} \begin{bmatrix} r_{11} & r_{12} & r_{13} & p_x \\ r_{21} & r_{22} & r_{23} & p_y \\ r_{31} & r_{32} & r_{33} & p_z \\ 0 & 0 & 0 & 1 \end{bmatrix} $$

$$ = \begin{bmatrix} cos\theta_1 r_{11} + sin\theta_1 r_{21} & cos\theta_1 r_{12} + sin\theta_1 r_{22} & . & . \\ -sin\theta_1 r_{11} + cos\theta_1 r_{21} & -sin\theta_1 r_{12} + cos\theta_1 r_{22} & . & . \\ r_{31} & r_{32} & . & . \\ 0 & 0 & . & . \end{bmatrix} $$

$$ \begin{bmatrix} . & . & cos\theta_1 r_{13} + sin\theta_1 r_{23} & cos\theta_1 p_x + sin\theta_1 p_y \\ . & . & -sin\theta_1 r_{13} + cos\theta_1 r_{23} & -sin\theta_1 p_x + cos\theta_1 p_y \\ . & . & r_{33} & p_z - L_1 \\ . & . & 0 & 1 \end{bmatrix} \tag{22} $$

The calculation on the right side of the equation in Equation 21 is shown in Equation 23.

$$ {}^{1}_{2}T . {}^{2}_{3}T . {}^{3}_{4}T = \begin{bmatrix} cos{\theta_2}^2 + sin{\theta_2}^2 & 0 & 0 & cos\theta_2 L_2 \\ 0 & 0 & 1 & L_3 \\ 0 & -sin{\theta_2}^2 - cos{\theta_2}^2 & 0 & -sin\theta_2 L_2 \\ 0 & 0 & 0 & 1 \end{bmatrix} \tag{23} $$

The equalization of the elements in the third column of the matrices in Equation 22 and Equation 23 to each other is shown in Equations 24-25-26. Using these equalizations, angle values are reached from the given position values Px, Py and Pz. If the equations are not sufficient, the calculations in Equation 22 are continued.

$$cos\theta_1 p_x + sin\theta_1 p_y = cos\theta_2 L_2 \quad (24)$$

$$-sin\theta_1 p_x + cos\theta_1 p_y = L_3 \quad (25)$$

$$p_z - L_1 = -sin\theta_2 L_2 \quad (26)$$

The process of squaring both sides of the equation in Equation 24 is shown in Equation 27.

$$(cos\theta_1 p_x + sin\theta_1 p_y)^2 + (-sin\theta_1 p_x + cos\theta_1 p_y)^2 = (cos\theta_2 L_2)^2 + (L_3)^2 \quad (27)$$

If the expression in Equation 19 is simplified and written instead of L2 and L3, Equation 28 is obtained.

$$(p_x)^2 + (p_y)^2 = (3.1945104 * 10\text{^}5)\ cos{\theta_2}^2 + 16641 \quad (28)$$

The equality in Equation 28 is solved by applying the trigonometric expression from Equation 10. As shown in Equation 29, the expression $\cos\theta$ is isolated to proceed with the solution. Thus, given the position values Px and Py, the amount of rotation required for the second axis (θ_2) is determined.

$$a = \cos\theta_2 = \sqrt{\frac{(p_x)^2 + (p_y)^2 - 16641}{3.1945104 * 10\text{^}5}}$$
$$\theta_2 = Atan2(\sqrt{1 - a^2}, a) \quad (29)$$

The amount of angular rotation of the first axis can be obtained from the equation in Equation 25. In solving this equation, the trigonometric expression in Equation 10 is applied. Equation 30 shows the solution steps.

$$-sin\theta_1 p_x + cos\theta_1 p_y = L_3 = 129 = c$$
$$a = P_x, b = P_y$$
$$\theta_1 = arctan2(a, b) + arctan(\pm\sqrt{a^2 + b^2 - c^2}, c) \quad (30)$$

2.6 Microcontroller (Arduino Uno) with Matlab Serial Communication

The robotic arm was controlled via serial communication between Matlab and the Arduino program. Movement commands and graphical processing for the robotic arm were handled through Matlab, while encoder data reading and PID control of the servo motors were managed by Arduino. The PID control of the motors was implemented using the Arduino library.

2.7 Determining PID Coefficients

The system response obtained with the values determined using the Ziegler-Nichols method was not satisfactory. Therefore, approximate kp, ki and kd values were found using trial and error. For the first axis, a value of 45° was used, and for the second axis, a value of -30° was considered. Some of the values used during the trials are shown in Table 4. By calculating the position differences for each axis, an error vector was created. Suitable kp, ki and kd values were found by minimizing the error vector.

Table 4: PID coefficients and system response

1.Eksen			2. Eksen			Sistem Cevabı									
45°			-30°												
Kp	Ki	Kd	Kp	Ki	Kd	Px-Teo. (XG) mm	Px-Den. (XD) mm	Px-Hata (mm)	Py-Teo. (XG) mm	Py-Den. (XD) mm	Py-Hata (mm)	Pz-Teo. (XG) mm	Pz-Den. (XD) mm	Pz-Hata (mm)	Hata Vektörü (mm)
0,0473	1E-05	1E-05	0,0253	1E-05	1E-05	254,896	256,614	1,718	437,329	437,449	0,12	805,6	803,855	-1,745	2,452
0,0473	3E-05	1E-05	0,0253	1E-05	1E-05	254,896	256,206	1,31	437,329	437,622	0,293	805,6	803,958	-1,642	2,121
0,0473	5E-05	1E-05	0,0253	1E-05	1E-05	254,896	256,022	1,126	437,329	437,73	0,401	805,6	803,958	-1,642	2,031
0,0473	6E-05	1E-05	0,0253	1E-05	1E-05	254,896	255,93	1,034	437,329	437,783	0,454	805,6	803,958	-1,642	1,993
0,0473	6E-05	5E-05	0,0253	1E-05	1E-05	254,896	255,93	1,034	437,329	437,783	0,454	805,6	803,958	-1,642	1,993
0,0473	6E-05	1E-04	0,0253	1E-05	1E-05	254,896	256,114	1,218	437,329	437,676	0,347	805,6	803,958	-1,642	2,074
0,0473	2E-04	1E-04	0,0253	1E-05	1E-05	254,896	254,646	-0,25	437,329	438,532	1,203	805,6	803,958	-1,642	2,051
0,0473	**1E-04**	**1E-04**	0,0253	1E-05	1E-05	**254,896**	**255,288**	**0,392**	**437,329**	**438,156**	**0,827**	**805,6**	**803,958**	**-1,642**	**1,880**
0,0473	1E-04	1E-04	0,0253	2E-05	1E-05	254,896	255,247	0,351	437,329	438,116	0,787	805,6	804,061	-1,539	1,764
0,0473	1E-04	1E-04	0,0253	3E-05	1E-05	254,896	255,297	0,401	437,329	438,021	0,692	805,6	804,164	-1,436	1,644
0,0473	1E-04	1E-04	0,0253	4E-05	1E-05	254,896	255,164	0,268	437,329	438,033	0,704	805,6	804,266	-1,334	1,532
0,0473	1E-04	1E-04	0,0253	5E-05	1E-05	254,896	255,122	0,226	437,329	437,991	0,662	805,6	804,369	-1,231	1,416
0,0473	1E-04	1E-04	0,0253	8E-05	1E-05	254,896	255,005	0,109	437,329	437,729	0,4	805,6	804,882	-0,718	0,829
0,0473	1E-04	1E-04	**0,0253**	**1E-04**	**1E-05**	**254,896**	**254,88**	**-0,016**	**437,329**	**437,604**	**0,275**	**805,6**	**805,19**	**-0,41**	**0,494**

2.8 Data Acquisition from the Encoder

The 14-bit encoder integrated into the back of the motor driver was configured to generate 30,000 pulses per revolution. When the desired angle values are entered into the system, the axes move simultaneously, and the axis that reaches the desired angle stops. To test the robotic arm, sample angle values were provided, and absolute error, relative error ratios, and standard deviations were calculated.

Table 5: Error values when the robot arm is given values of 45° to the first axis and -45° to the second axis, and this process is set to 10 repetitions

Experiment-1	θ_1	θ_2	Px	Py	Pz
Real value	45,000	-30,000	254,896	437,330	805,600
Average value	45,021	-29,995	254,753	437,441	805,557
Absolute error (min.)	0,010	0,000	0,007	0,054	0,000
Absolute Error (Max.)	0,040	0,040	0,375	0,184	0,342
Relative error (min.)	0,022	0,000	0,003	0,012	0,000
Relative error (max.)	0,089	-0,134	0,147	0,042	0,043
Standard deviation	0,011	0,019	0,145	0,033	0,162

Table 6: Error values when the robot arm is given values of 45° to the first axis and -45° to the second axis, and this process is set to 30 repetitions

Experiment-2	θ_1	θ_2	Px	Py	Pz
Real value	45,000	-45,000	191,383	373,817	922,657
Average value	45,006	-45,051	191,094	373,587	923,010
Absolute error (min.)	0,000	0,000	0,016	0,016	0,000
Absolute Error (Max.)	0,040	0,140	0,952	0,559	0,975
Relative error (min.)	0,000	0,000	0,008	0,004	0,000
Relative error (max.)	0,089	-0,310	0,500	0,150	0,106
Standard deviation	0,014	0,046	0,315	0,180	0,317

The average, absolute error, relative error, and standard deviation values of the angle measurements from the encoder and the position values of the end-effector calculated based on these angle values are shown in Table 5 and Table 6.

III. RESULTS AND RECOMMENDATIONS

In this study, the design, manufacturing, and experimental work of a two-axis, spherical trajectory-tracing robotic arm with a special end-effector were carried out. The pneumatic end-effector was designed to grasp spherical and ear-shaped objects. Additionally, a pulley system was designed between the end-effector and the second axis to maintain the parallelism of the end-effector with the ground. This setup allowed the object to be transported to the desired point while maintaining its stance position. The added pulley system effectively acted as a third axis, thus saving on axis and motor usage by utilizing the servo motor on the second axis as an actuator.

The forward and inverse kinematic calculations determined the coordinates to which the robotic arm would move given angle values for the axes, or the angles needed to reach a given coordinate by the end-effector. These calculations were validated with sample angle values. The validated calculations were embedded into the Matlab interface, and a command screen was created. The system's successful operation was observed when sample angle values were provided.

During the experimental phase, it was observed that the deviation and error values of the sample angle values and repeated movements indicated that the process or operation would not require extremely high precision. Based on these deviation values, it is recommended that the robotic arm be used for operations requiring medium precision. However, it can be stated that these errors and deviations would be significantly reduced if surface tolerances, bearing tolerances, and manufacturing defects were corrected. Moreover, by selecting appropriate PID values and adjusting motor characteristics, deviations in the trajectory can be optimized. The most suitable PID values were attempted to be determined using the Ziegler-Nichols method; however, the system response obtained with these values was not satisfactory. Therefore, approximate kp, ki and kd values were found by adding and subtracting to the determined PID values.

A precise design capable of operating within high tolerances can be achieved by selecting an appropriate control interface and control method for the robotic arm.

For repeated movements, the standard deviations of 10 and 30 repetitions ranged from 7.4% to 17.4%, indicating that adjustments are needed during the manufacturing and sizing of the robotic arm. For these deviation values to be suitable for precise work, manufacturing and assembly errors must be eliminated. In similar studies, it has been observed that these deviation values were around 0.1%.

The robotic arm and end-effector were designed focusing on a specific material. However, material optimization or using different materials might also achieve the same functionality. Since the motors and reducers provided by the BAP research project were used in this study, dimensional optimization was not addressed. A robotic arm and end-effector design suitable for a specific working area was made, and a material was selected that would not require strength calculations. If material optimization and suitable material selection are carried out, peaks in the acceleration-time graph during the robotic arm's movement will not be observed.

REFERENCES

[1]. Adalı, Ş. (2001). 3-boyutlu Robot Simülasyonu. (Yüksek Lisans Tezi). https://polen.itu.edu.tr/handle/11527/10668

[2]. Adar, N. G., Ören, H., & Kozan, R. (5). 5 Serbestlik dereceli robot kolunun modellenmesi ve kontrolü. Sakarya University Journal of Science, 17(1), 155-160.

[3]. Ben-Ari, M., & Mondada, F. (2017). Elements of robotics. Springer Nature.

[4]. Bejczy, A. K., & Paul, R. P. (1981, December). Simplified robot arm dynamics for control. In 1981 20th IEEE Conference on Decision and Control including the Symposium on Adaptive Processes (pp. 261-262). IEEE.

[5]. Bernier, C. (t.y.). How Pneumatic End Effectors Work? Robotiq. https://blog.robotiq.com/bid/65604/How-Pneumatic-End-Effectors-Work

[6]. Bingül, Z. ve Küçük, S. (2017a). Robot Kinematiği (3.). Umuttepe Yayınları.

[7]. Bingül, Z. ve Küçük, S. (2017b). Robot Dinamiği ve Kontrolü (2.). Umuttepe Yayınları.

[8]. Cao, Y., Lu, K., Li, X., & Zang, Y. (2011). Accurate numerical methods for computing 2d and 3d robot workspace. International Journal of Advanced Robotic Systems, 8(6), 76.

[9]. Chen, W. H., Chen, C. P., Tsai, J. S., Yang, J., & Lin, P. C. (2013). Design and implementation of a ball-driven omnidirectional spherical robot. Mechanism and Machine Theory, 68, 35-48.

[10]. Controlling a KUKA Industrial Robot Using a SIMATIC S7-1500. (t.y.). https://docplayer.net/47895646-Controlling-a-kuka-industrial-robot-using-a-simatic-s7-1500.html

[11]. Diouf, A., Belzile, B., Saad, M., & St-Onge, D. (2024). Spherical rolling robots—Design, modeling, and control: A systematic literature review. Robotics and Autonomous Systems, 104657.

[12]. Eren, O. ve Kaftanoğlu, B. (2001). Altı Serbestlik Dereceli Bir Endüstriyel Robotun Tasarımı İmalatı ve Çalıştırılması. Makina Tasarım ve İmalat Dergisi, 4(2), 103-111.

[13]. Samadikhoshkho, Z., Zareinia, K., & Janabi-Sharifi, F. (2019, May). A brief review on robotic grippers classifications. In 2019 IEEE Canadian Conference of Electrical and Computer Engineering (CCECE) (pp. 1-4). IEEE.

[14]. Hartenberg, R. S. ve Denavit, J. (1955). A Kinematic Notation for Lower-Pair Mechanisms Based on Matrices, 215-221.

[15]. Industrial Robots. (t.y.).Distrelec. 17 Şubat 2020, https://www.distrelec.de/en/industrial-robots/cms/knowhow-industrial-robots

[16]. Kumar, V. (2010). 50 Years of Robotics [From the Guest Editors]. IEEE Robotics Automation Magazine, 17(3), 8-8. doi:10.1109/MRA.2010.938493

[17]. Mustafa, A. M. ve Al-Saif, A. (2014). Modeling, Simulation and Control of 2-R Robot. Global Journals Inc. (USA), 14(1), 49-54.
[18]. Pneumatic Cylinders. (t.y.).Tameson. https://tameson.com/pneumatic-cylinders.html?id_country=211
[19]. Öztürk, M. (2014). Antropomorfik Robotların Dinamiği ve Adaptif Kontrol Uygulamaları: Matlab/simulink Modelleme.
[20]. Saygılı, Ç. (2006, 1 Aralık). Scara Tipi Bir Robotun Tasarımı ve Animasyonu. (Yüksek Lisans Tezi). http://acikerisim.selcuk.edu.tr:8080/xmlui//handle/123456789/7333
[21]. Servo Motor Technology. (t.y.). Oriental Motor. https://www.orientalmotor.com/servo-motors/technology/servo-motor-overview.html#
[22]. Spong, M. W., Hutchinson, S. ve Vidyasagar, M. (2004). Robot Dynamics and Control (2.).
[23]. Siciliano, B., Sciavicco, L., Villani, L. ve Oriolo, G. (2009). Robotics: Modelling, planning and control. London: Springer.
[24]. Teach Pendants Information. (t.y.). Engineering 360 https://www.globalspec.com/learnmore/motion_controls/operator_interfaces/teach_pendants
[25]. Tonbul, T. ve Sarıtaş, M. (2013). Beş Eksenli Bir Edubot Robot Kolunda Ters Kinematik Hesaplamalar ve Yörünge Planlaması. Gazi Üniversitesi Mühendislik Mimarlık Fakültesi Dergisi, 18(1), 145-167.
[26]. Yavuz, E., Alıcı, M. ve Uyar, E. (2015). 3 Serbestlik Dereceli (3R) Bir Robot Manipülatörünün Kontrolü ve Görüntü İşlemeye Dayalı Nesne Taşınması Control of 3 DOF (3R) Robot Manipulator and Moving Objects Based on Image Processing (ss. 654-659). Otomatik Kontrol Ulusal Toplantısı.